Journal of Directed Energy, **3**, Summer 2010, 320–342

Methodology for Reflected Laser Beam Hazard Analyses

Edward Early* and George Megaloudis
TASC, Brooks City-Base, Texas 78235

and

Paul Kennedy and Robert J. Thomas
U.S. Air Force Research Laboratory, 711HPW/RHDO, Brooks City-Base, Texas 78235

Previous reflected laser beam hazard evaluations have been based primarily on simplifying and overly conservative assumptions. In the case of high-energy-laser (HEL) field tests, such assumptions typically produce reflected nominal ocular hazard distance (RNOHD) results that cannot be contained within the boundaries of existing test ranges. This severely limits the ability to test HEL systems under operational conditions. A methodology was developed to address the need of the laser safety community for a more rigorous and accurate procedure to determine RNOIIDs to support HEL field tests. The methodology consists of several physically based models and is applicable to scenarios in which a single laser illuminates a target while both move along independent trajectories. The salient features of the methodology are consideration of reflections only in the specular direction, the use of reflecting properties of actual materials, and calculation of exposure times for specific engagement scenarios. The equations and procedures of the methodology are demonstrated using an example engagement scenario.

KEYWORDS: Beam propagation, Exposure time, High-energy laser, Irradiance, Laser safety, Reflected beam, Reflected nominal ocular hazard distance (RNOHD)

Nomenclature

D_{r1}	effective $1/e$ diameter of the reflected beam
D_{t1}	incident beam $1/e$ diameter at the target
D_{01}	incident beam $1/e$ diameter on the laser exit aperture
D_1	incident beam $1/e$ diameter
$D_{1\parallel}$	reflected beam $1/e$ diameter parallel to the target axis of symmetry
$D_{1\perp}$	reflected beam $1/e$ diameter perpendicular to the target axis of symmetry
D_2	reflected beam $1/e^2$ diameter used to calculate exposure time
E_r	reflected irradiance
E_{0r}	reflected on-axis irradiance
F	laser system focal length

Received June 28, 2010; revision received August 18, 2010.
*Corresponding author; e-mail: Edward.early@tasc.com.

$\hat{\boldsymbol{k}}_i$ unit vector pointing in the incident direction
$\hat{\boldsymbol{k}}_r$ unit vector pointing in the reflected direction
$\hat{\boldsymbol{L}}$ axis unit vector of a cylinder or cone
M^2 beam quality
$\hat{\boldsymbol{n}}$ surface normal unit vector at the center of the illuminated region
P target surface radius of curvature
R distance from the target measured along the propagation direction of the reflected beam
r distance from laser exit aperture measured along the beam propagation direction
$\boldsymbol{r}_L$ laser position vector
$\boldsymbol{r}_O$ observer position vector
$\boldsymbol{r}_T$ target position vector
S Strehl ratio
T exposure duration
$\boldsymbol{v}_E$ observer velocity minus the reflected beam velocity
$\boldsymbol{v}_L$ laser velocity
$\boldsymbol{v}_O$ observer velocity
$\boldsymbol{v}_R$ reflected beam velocity as a function of position along the reflected propagation direction
$\boldsymbol{v}_T$ target velocity
α angle between $\mathbf{v}_E$ and the reflected beam propagation direction
β angle of incidence or reflection
γ cone half-angle
θ angle between incident direction and target axis
λ laser wavelength
μ atmospheric attenuation coefficient
Φ laser power
ϕ_b $1/e$ full-angle beam divergence of the incident beam
ϕ_c contribution to the $1/e$ full-angle divergence of the reflected beam due to target surface curvature
ϕ_{ce} $1/e$ full-angle reflected beam divergence due to curvature used to calculate the exposure time
ϕ_{c1} $1/e$ full-angle reflected beam divergence due to curvature used to calculate the reflected irradiance
ϕ_m contribution to the $1/e$ full-angle divergence of the reflected beam due to target surface bidirectional reflectance distribution function
ϕ_1 $1/e$ full-angle reflected beam divergence
$\phi_\parallel$ reflected beam $1/e$ divergence in the plane containing the target axis of symmetry
$\phi_\perp$ reflected beam $1/e$ divergence in the plane perpendicular to the target axis of symmetry

1. Introduction

High-energy-laser (HEL) systems developed for outdoor military applications present formidable challenges for laser safety analyses.[1,2,6–10] In addition to the obvious hazard from exposure to the direct beam, exposure to the beam reflected by the illuminated target can also pose hazards due to the high laser power.[3–5] These hazards can severely limit the

ability to test HEL systems. These tests are performed on ranges with controlled access so that personnel can be excluded from designated hazard zones on the surface and in the air. A planned HEL test is conducted only if the hazard zones are contained entirely within the controlled surface and airspace boundaries of the range for all test conditions. Thus, the primary goal of laser safety analyses performed prior to the execution of a HEL system test is to quantify the spatial extent and location of reflected beam hazard zones and ensure that they are contained within the test range boundaries. A hazard zone is a three-dimensional region around a target, whereas a hazard distance applies to a specific direction. A hazard zone is typically constructed by determining the longest hazard distance and using this as the radius for a hazard zone sphere centered on the target.

The hazard distance for laser reflections is defined as the distance from the target at which the irradiance of the reflected beam equals the maximum permissible exposure (MPE) (Ref. 2); this distance is termed the reflected nominal ocular hazard distance (RNOHD). Determining the RNOHD requires knowledge of the reflected beam characteristics and the MPE. The former depends primarily on the incident beam and the reflecting properties of the target surface material. The MPE depends on wavelength and exposure time and decreases with increasing exposure time. The mathematical complexity of estimating the RNOHD for a given engagement scenario often leads laser safety analysts to base the hazard calculations on overly conservative assumptions. In general, such overly conservative assumptions, sometimes referred to as worst case, often lead to an unnecessarily large RNOHD that can severely constrain the HEL test plan or delay the execution of a field test.

The methodology presented in this paper was developed to provide a unified framework for calculating a more accurate RNOHD than can be obtained with overly conservative assumptions. The salient features of this methodology are consideration of reflections only in the specular direction, use of reflecting properties of actual materials, and calculation of exposure times for the specific engagement scenario. The overly conservative approach treats the target material as a perfect reflector and often neglects the curvature of the illuminated portion of the target. This approach also assumes an exposure time of 10 s, which results in the smallest MPE and hence the longest RNOHD. In contrast, the methodology presented here incorporates the actual shape and reflecting properties of the target, the latter given by the bidirectional reflectance distribution function (BRDF),[5] and an exposure time model based on the geometry of the engagement scenario, involving locations, velocities, and orientations of the HEL and the illuminated target. As a consequence, this methodology does not overestimate the reflected irradiance and exposure time as is the case when overly conservative assumptions are applied. Thus, the methodology leads to a shorter RNOHD that is more manageable for test ranges.

The reflected laser beam hazard analysis methodology presented in this paper is summarized in Sec. 2. The methodology consists of several physically based models and is applicable to engagement scenarios in which a single laser illuminates a target with both laser and target possibly moving along independent trajectories. The beam propagation model presented in Sec. 3 is used to calculate the properties of the incident beam at the target location. The reflected irradiance model combines the properties of the incident beam, the target shape, and the BRDF of the target surface material and is presented in Sec. 4. The exposure time model detailed in Sec. 5 takes into account the time-varying position, velocity, and orientation of both the target and laser, as well as the motion of the reflected beam. The methodology is demonstrated in Secs. 6 and 7 by calculating the RNOHD for an engagement scenario involving planar, cylindrical, and conical targets.

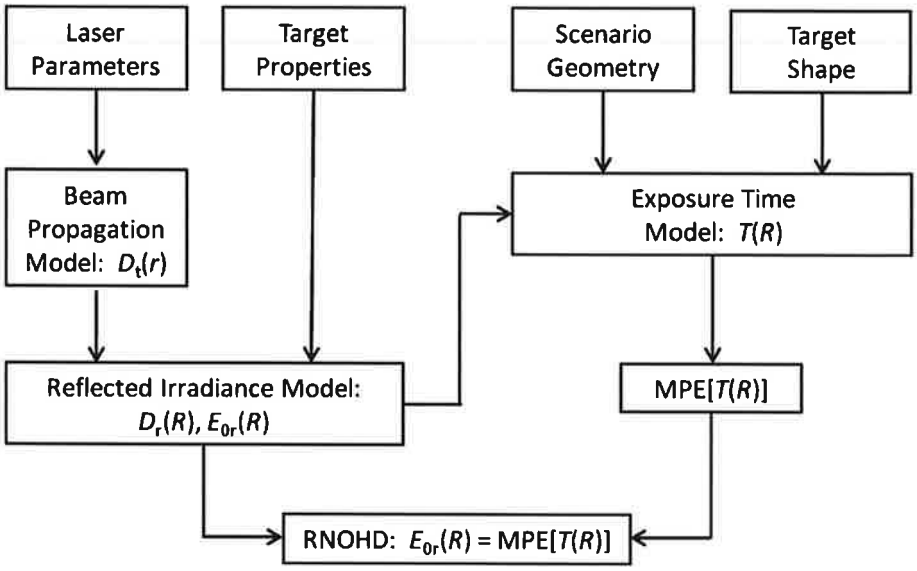

Fig. 1. Principal components of the methodology used to compute the RNOHD.

2. Methodology Overview

The purpose of the methodology is to calculate the RNOHD, which depends on both the reflected irradiance E_r and the MPE. The reflected irradiance depends on the distance R from the target, whereas the MPE depends on the exposure time T, defined as the time interval during which laser radiation reflected by the target illuminates the location of an observer. As discussed in Sec. 5, the exposure time also depends on R. For a given wavelength and T, the MPE is specified in the ANSI Z136.1 safety standard.[1] Therefore, the RNOHD is calculated by finding the solution to the equation

$$E_r(R) = \text{MPE}\,[T(R)]. \tag{1}$$

The principal components of the methodology used to compute the RNOHD are depicted in Fig. 1. The majority of the required calculations are performed by the beam propagation, reflected irradiance, and exposure time models discussed in detail in Secs. 3, 4, and 5, respectively. All of the necessary equations for these models are presented in this paper and have been implemented in a stand-alone code for calculating the RNOHDs for user-specified engagement scenarios.

The beam propagation model uses laser system parameters to calculate the diameter of the beam incident on the target D_t and the resulting incident irradiance distribution. The reflected irradiance model uses the output of the beam propagation model and the target surface properties, such as the shape and BRDF, to calculate both the diameter D_r and the on-axis irradiance E_{0r} of the beam reflected in the specular direction as a function of the distance R from the target. The on-axis irradiance is calculated from a closed-form expression that is valid when the laser beam illuminates a planar, cylindrical, or conical region on the target surface.

Inputs to the exposure time model include laser, target, and observer locations, velocities, and orientations. The model is applicable for planar, cylindrical, and conical target shapes;

accounts for the relative motion between the laser and target; and calculates the velocity and propagation direction of the reflected beam at discrete times in the scenario. These quantities are used to calculate the exposure time as a function of distance from the target along the direction of specular reflection. It follows that the MPE, which depends on the exposure time, is also a function of distance from the target along the direction of specular reflection. The resulting reflected irradiance and MPE are used in Eq. (1) to calculate the RNOHD.

3. Beam Propagation Model

The beam propagation model calculates both the irradiance and diameter of the laser beam incident on the target surface, and these quantities are subsequently used in the reflected irradiance model to calculate the properties of the reflected beam. In some applications, the laser beam has a waist at the exit aperture of the system and diverges with increasing range. In contrast, most HEL beams are focused at the target range and therefore converge to an external waist. Focusing the beam at the target range maximizes the irradiance on the target. This section presents a beam propagation model that applies to both focused and unfocused laser beams.

The reflected irradiance model requires the beam diameter at the target, so an expression for the beam size as a function of distance from the laser is necessary. If the beam diverges at the system exit aperture, then the aperture is often the location of the beam waist. In this case, the $1/e$ laser beam diameter D_1 at a distance r from the laser is given by

$$D_1^2(r) = D_{01}^2 + \phi_b^2 \cdot r^2, \tag{2}$$

where D_{01} is the $1/e$ beam diameter at the exit aperture and ϕ_b is the $1/e$ full-angle beam divergence. In contrast, a focused laser beam converges to the location of the beam waist and then diverges at longer distances.

The beam propagation model calculates the irradiance distribution of a focused beam on a plane perpendicular to the direction of propagation as a function of the distance from the exit aperture of the laser system. This model is used primarily to determine beam parameters on the target surface that are required by the reflected irradiance model. The beam propagation model includes the effects of nonideal beam quality and imperfect compensation of atmospheric turbulence effects on the propagating beam if adaptive optics are included in the system.

The $1/e$ beam diameter of a focused beam is given by

$$D_1^2(r) = D_{01}^2 \left[\left(1 - \frac{r}{F}\right)^2 + \left(\frac{2}{\pi}\frac{\lambda}{D_{01}^2} M^2 \cdot r\right)^2 \right], \tag{3}$$

where F is the focal length, λ is the wavelength, and M^2 is the beam quality. The beam irradiance in a plane perpendicular to the propagation direction is then given by

$$E(r, \zeta) = \frac{4}{\pi} \frac{\Phi}{D_1^2(r)} \exp\left[\frac{-4\zeta^2}{D_1^2(r)}\right] \exp(-\mu \cdot r) \cdot S, \tag{4}$$

where Φ is the beam power, ζ is the transverse distance from the beam axis, μ is the atmospheric attenuation coefficient, and S is the Strehl ratio (for turbulence-compensated systems). The on-axis irradiance $E_0(r)$ is given by substituting $\zeta = 0$ into Eq. (4).

4. Reflected Irradiance Model

The reflected irradiance model consists of closed-form expressions that quantify the diameter and on-axis irradiance of the laser beam reflected in the specular direction as a function of distance from the target. The $1/e$ diameter D_{r1} of the reflected beam increases with the distance R from the target, and the reflected on-axis irradiance E_{0r} is given by

$$E_{0r}(R) = \frac{4}{\pi} \frac{\rho \cdot \Phi}{D_{r1}^2(R)}, \tag{5}$$

where ρ is the reflectance of the target material ($0 \leq \rho \leq 1$).

In general, assuming a specular reflection, the $1/e$ beam diameter D_{r1} at a distance R from the target is given by

$$D_{r1}^2(R) = D_{t1}^2 + \phi_1^2 \cdot R^2, \tag{6}$$

where D_{t1} is the $1/e$ diameter of the incident beam at the target and ϕ_1 is the $1/e$ full-angle reflected beam divergence. The diameter of the incident beam D_{t1} is given by Eq. (2) for an unfocused beam or Eq. (3) for a focused beam by setting r to the distance between the laser and the target. The reflected beam divergence has three components—ϕ_b due to the incident beam divergence, ϕ_m due to the BRDF of the target material, and ϕ_c due to the curvature of the target. These components are assumed to be additive, so that

$$\phi_1 = \phi_b + \phi_m + \phi_c. \tag{7}$$

The first two components are present for any beam and target material, whereas the presence of the last component depends on the shape of the target. The divergence of the reflected beam, for a converging incident beam, is illustrated in Fig. 2 for the planar, cylindrical, and conical target shapes considered in this paper. The transverse shape of the resulting reflected beam from each target shape is also shown in Fig. 2. The assumption of additive divergence components is based on geometrical optics.

4.1. Divergence due to incident beam

The calculation of D_{t1} and ϕ_b depends on the laser system. For a diverging beam with its waist at the system exit aperture, ϕ_b is specified as a system parameter and D_{t1} is calculated using Eq. (2) by setting r to the distance to the target. For a focused beam, D_{t1} is calculated similarly using Eq. (3). For a system with focal length F, the $1/e$ full-angle beam divergence is given by

$$\phi_b = \frac{2}{\pi} \frac{1}{\omega} \frac{\lambda}{D_{01}} M^2, \tag{8}$$

where

$$\omega = \frac{F}{\sqrt{F^2 + \left(\frac{Z_R}{M^2}\right)^2}}, \tag{9}$$

and

$$Z_R = \frac{\pi}{2} \frac{D_{01}^2}{\lambda} \tag{10}$$

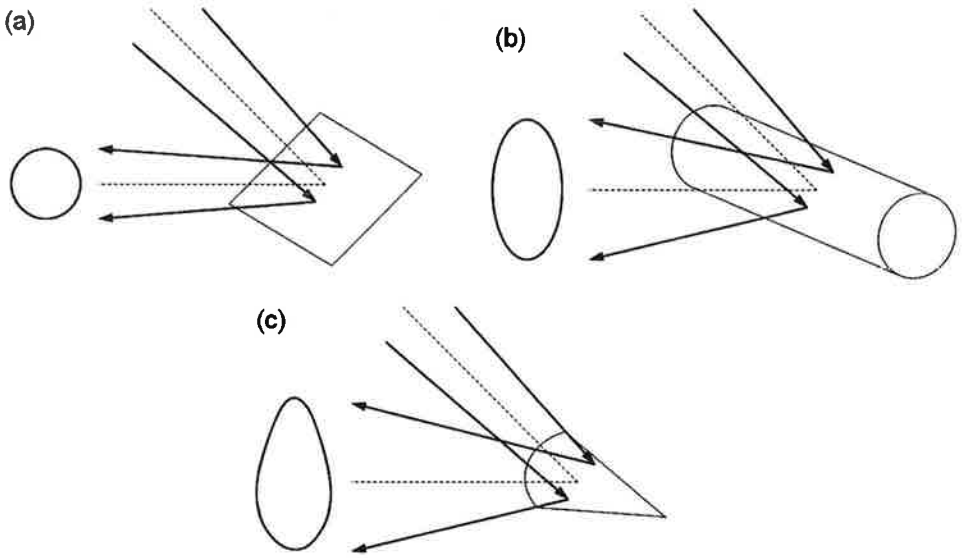

Fig. 2. Illustration of the reflected divergence and transverse shape for (a) planar, (b) cylindrical, and (c) conical target shapes for a circular incident beam. The central axes of the incident and reflected beams are denoted by the dashed lines.

is the Rayleigh range. Note that when Z_R is much larger than F, $\omega = FM^2/Z_R$ and $\phi_b = D_{01}/F$, as expected from simple geometrical considerations.

4.2. Divergence due to target material

The reflecting properties of a target material are quantified by the BRDF,[5] which includes the effects of surface roughness. In general, as the surface roughness decreases, the angular width of the lobe of the BRDF around the specular direction decreases and the value of the peak BRDF increases. The measured BRDF of a material with a relatively low surface roughness is shown in Fig. 3. For an angle of incidence of 30 deg, there is a sharp, distinct peak in the BRDF in the specular direction, i.e., at an angle of reflection of 30 deg.

There are several methods to quantify the effect of the BRDF on the reflected beam divergence, and all rely on measurements. Specialized equipment is used to measure the BRDF with the high angular resolution required for materials with a peaked BRDF in the specular direction. One method is to obtain the divergence directly from the measured BRDF. Using the data shown in Fig. 3, the angles at which the BRDF is $1/e$ of its maximum value, from interpolation, occur at 29.91 and 30.12 deg. Therefore, the full-angle beam divergence ϕ_m is 0.21 deg, or 3.7 mrad.

A second method is to fit a BRDF model to the data. With this method, ϕ_m is given by the full angular width at which the fitted BRDF model is reduced to $1/e$ of its peak value. For example, for a material similar to that shown in Fig. 3, the estimated value of ϕ_m is 0.15 deg, or 2.5 mrad.

The normalized BRDFs of several materials are shown in Fig. 4. Despite the differences in materials and surface appearance, all of them have approximately the same width of the BRDF around the specular direction, corresponding to $\phi_m = 2.5$ mrad. The differences between materials are evident in the value of the BRDF at angles removed from the specular

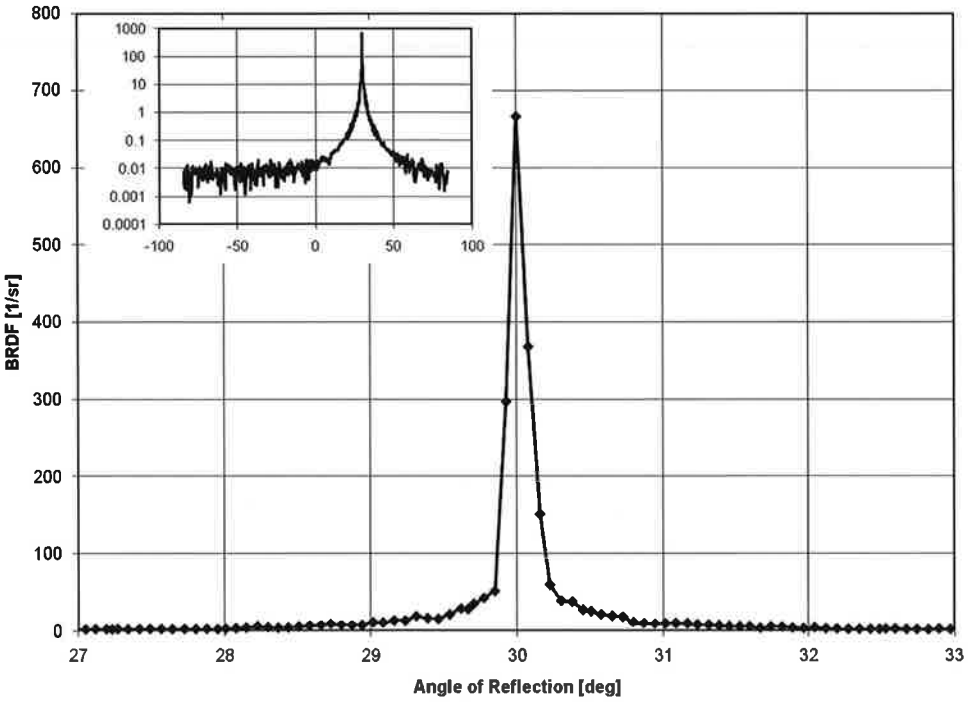

Fig. 3. BRDF as a function of reflected angle measured for 2024 aluminum at an angle of incidence of 30 deg. The inset has an expanded angle scale and a logarithmic BRDF scale.

direction (0 deg in Fig. 4). For the materials shown in Fig. 4, the BRDF at an angle of 1 deg from the specular direction decreases by approximately four orders of magnitude as the material becomes more polished. In addition, the peak value of the BRDF increases from 1,330 sr^{-1} for 2024 aluminum to 423,000 sr^{-1} for mirror aluminum. These data imply that, for metallic materials, the divergence due to the target material is approximately constant despite differences in the peak BRDF and its decrease in magnitude at angles removed from the specular direction.

In most cases, the BRDF of the target material for a specific engagement is not known. In these cases, a conservative estimate for ϕ_m is required. The peak reflected irradiance is proportional to ϕ_m^{-2}, whereas the exposure time is proportional to ϕ_m [from Eq. (19) below]. The proportionality of MPE with exposure time T varies from $T^{-1/4}$ to T^{-1}, depending on wavelength and exposure time, and therefore has the same proportionality with ϕ_m as it does with T. Although both the peak reflected irradiance and the MPE increase as ϕ_m decreases, the stronger dependence of the former implies that a smaller ϕ_m is more conservative. Because many of the targets involved in HEL field tests are metallic, and even if they are painted the base metal is exposed upon heating, a value of $\phi_m = 2.5$ mrad is taken as a conservative estimate based on the results shown in Fig. 4. As more BRDF data become available, this value of ϕ_m may change.

4.3. Divergence due to target shape

The third contribution to the divergence of the reflected beam arises from the shape of the target. For a planar target, the shape contributes nothing to the divergence because there

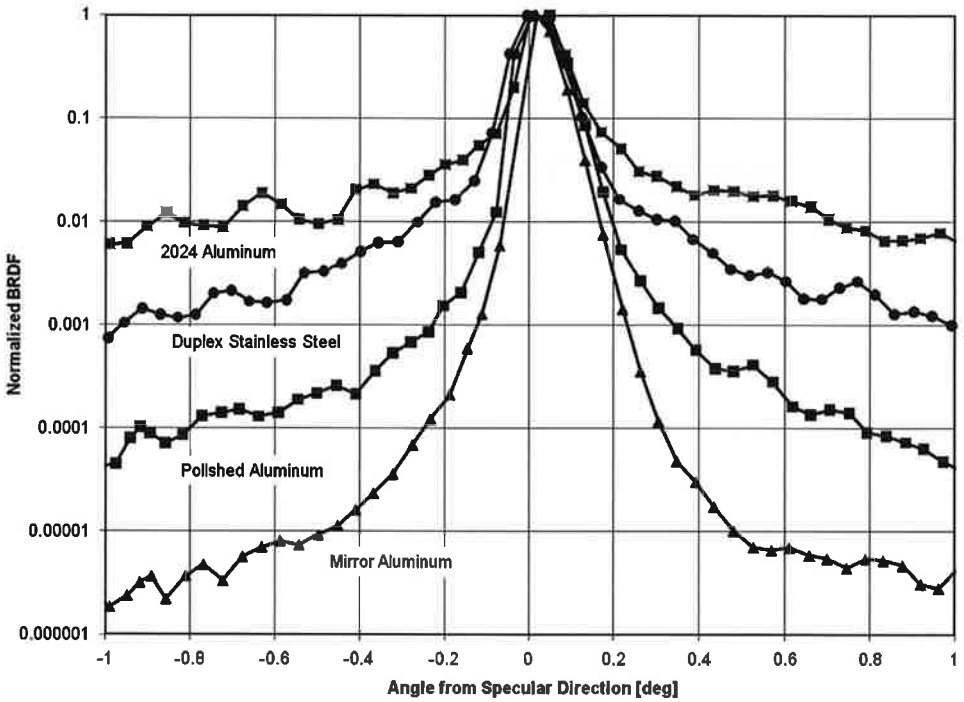

Fig. 4. Normalized BRDF as a function of angle from the specular direction for the indicated materials at an angle of incidence of 5 deg.

is no curvature—a circular incident beam ($1/e$ locations transverse to the central axis form a circle) remains a circular beam upon reflection, as illustrated in Fig. 2. However, for cylindrical and conical targets, a circular incident beam is modified upon reflection, again as illustrated in Fig. 2. For a cylindrical target (a fairly common situation), the reflected beam is elliptical. The portion of the beam parallel to the axis of the cylinder contributes nothing to the divergence of the reflected beam due to target shape, whereas the portion perpendicular to the axis contributes divergence due to the target curvature. The reflected beam for a conical target is egg-shaped due to the changing radius of curvature along the axis of the cone.

Both the on-axis reflected irradiance, calculated using Eq. (5), and the exposure time, calculated using Eq. (19) below, require the diameter of the reflected beam. However, the divergence due to curvature must be calculated differently in each case. The geometry for reflection by a cylindrical target is illustrated in Fig. 5, where the incident beam is assumed to have a planar wavefront and the incident beam central axis intersects the axis of the cylinder. For an incident ray along the central axis, indicated by the horizontal dashed line, the reflected ray is also along the central axis. For an incident ray offset from the central axis by a distance ζ, the angle $\theta = \sin^{-1}(\zeta/P)$, where P is the radius of curvature of the cylindrical target, and the resulting reflected ray makes an angle of 2θ with the central axis.

The reflected beam has a spherical wavefront in a plane perpendicular to the cylinder axis, so the $1/e$ full-angle divergence of the reflected beam due to curvature, ϕ_{c1}, used to

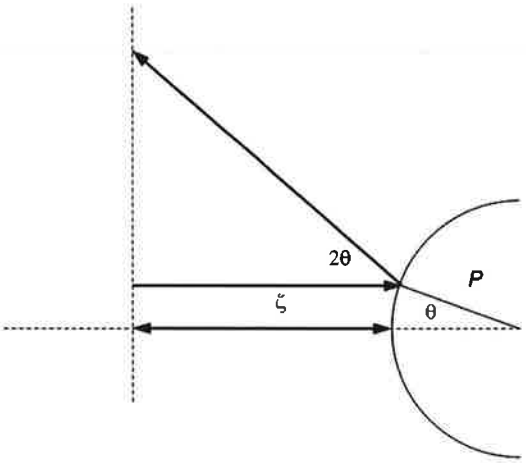

Fig. 5. Geometry of incident and reflected beams for a cylindrical target shape for rays both along and offset from the central axis (indicated by the horizontal dashed line).

calculate the reflected irradiance is given by

$$\phi_{c1} = 4\sin^{-1}\left(\frac{D_{t1}}{2P}\right), \tag{11}$$

where D_{t1} is the $1/e$ beam diameter at the target obtained from the beam propagation model. Referring to Fig. 5, $\sin\theta = \zeta/P$, so replacing ζ by $D_{t1}/2$ and recognizing that the reflected angle is 2θ and that the full-angle reflection adds another factor of two yields Eq. (11).

To calculate the exposure time, the irradiance of the reflected beam must be calculated for locations offset from the central axis because the beam sweeps over the observer location. Referring to Fig. 5, the distance from the target to the vertical dashed line is greater for the reflected ray offset from the central axis than it is for the ray on the central axis. Far from the target, the reflected irradiance varies inversely as the distance squared. It follows from Fig. 5 that at these distances the reflected irradiance is proportional to $\cos^2(2\theta)$. Therefore, for an incident beam with an exponential irradiance distribution, the dependence of the reflected irradiance on θ and ζ is given by

$$E(R) \propto \cos^2(2\theta)\cdot\exp\left[-\left(\frac{\zeta}{\zeta_1}\right)^2\right], \tag{12}$$

where $\zeta_1 = D_{t1}/2$ is the $1/e$ distance of the incident beam irradiance distribution. The effect of the $\cos^2(2\theta)$ term in Eq. (12) is to reduce the reflected beam divergence at which the irradiance is $1/e$ of its on-axis value, yielding the $1/e$ full-angle beam divergence ϕ_{ce}. The appropriate beam diameter to use to calculate ϕ_{ce} is found by solving the right-hand side of Eq. (12) for the value of ζ/P for which $E(R)$ has a value of $1/e$. The result is

$$\frac{\zeta}{P} = \begin{cases} \dfrac{\zeta_1}{P} & \text{for} \quad 0 \le \dfrac{\zeta_1}{P} < 0.1 \\ -0.0129 + 1.2317\left(\dfrac{\zeta_1}{P}\right) - 1.2802\left(\dfrac{\zeta_1}{P}\right)^2 + 0.4742\left(\dfrac{\zeta_1}{P}\right)^3 & \text{for} \quad 0.1 \le \dfrac{\zeta_1}{P} \le 1 \end{cases} \tag{13}$$

and ϕ_{ce} is given by

$$\phi_{ce} = 4\sin^{-1}\left(\frac{\zeta}{P}\right). \tag{14}$$

The situation is more complicated for a conical target, because the radius of curvature changes along the length of the cone and this affects the shape of the reflected beam, as illustrated in Fig. 2. In this case, ϕ_c is calculated approximately in the same manner as the divergence of the beam reflected by a cylindrical target but with the radius of curvature taken at the center of the illuminated region on the cone surface.

4.4. Reflected beam diameter and irradiance

Substituting Eq. (7) into Eq. (6) and considering the shape of the target, the beam diameters as a function of distance from the target are given by

$$D_{1//}^2(R) = D_{t1}^2 + (\phi_b + \phi_m)^2 R^2 = D_{t1}^2 + \phi_{//}^2 \cdot R^2, \tag{15}$$

$$D_{1\perp}^2(R) = D_{t1}^2 + (\phi_b + \phi_m + \phi_c)^2 R^2 = D_{t1}^2 + \phi_{\perp}^2 \cdot R^2, \tag{16}$$

where // and $\perp$ indicate directions parallel and perpendicular, respectively, to the axis of the cylinder or cone, and the appropriate value of ϕ_c is used (ϕ_{c1} for reflected irradiance, ϕ_{ce} for exposure time). The effective $1/e$ diameter of the reflected beam is then given by

$$D_{r1} = \sqrt{D_{1//} \cdot D_{1\perp}}. \tag{17}$$

Substituting Eqs. (15) and (16) into Eq. (5) yields the closed-form expression for the on-axis reflected irradiance as a function of distance from the target, considering the contributions to the divergence of the reflected beam from the laser system, material BRDF, and target curvature. For distances at which the diameter of the illuminated area on the target is inconsequential, the reflected irradiance is given by

$$E_{0r}(R) = \frac{4}{\pi}\frac{\rho \cdot \Phi}{\phi_{//} \cdot \phi_{\perp} \cdot R^2}. \tag{18}$$

5. Exposure Time Model

As illustrated in Fig. 1, one set of calculations of the methodology determines the reflected irradiance as a function of distance from the target. The other set calculates the MPE, which requires the exposure time. The exposure time model uses the diameter of the reflected beam and the geometrical specifics of the engagement scenario to determine the exposure time T, which is given by

$$T = \frac{D_2}{v_E \sin\alpha}, \tag{19}$$

where D_2 is the $1/e^2$ diameter of the reflected beam at the observer location, v_E is the magnitude of the difference vector $\boldsymbol{v}_E$ between the observer velocity and the velocity

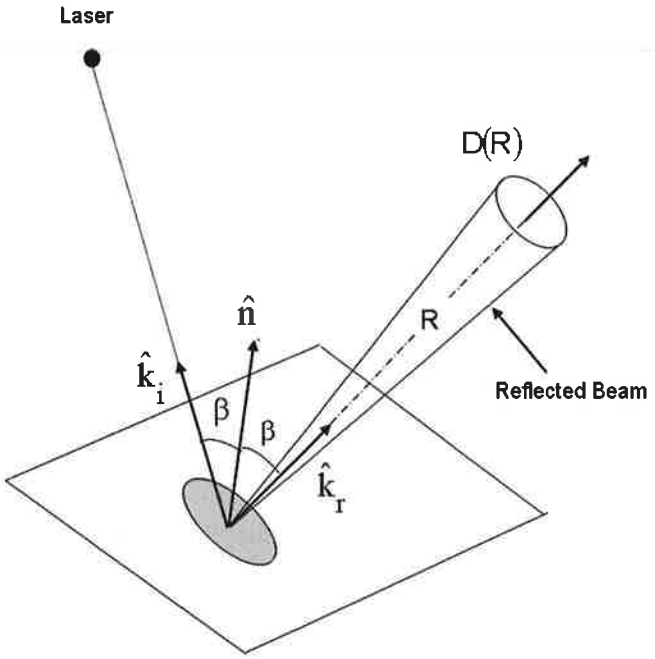

Fig. 6. Geometry for the exposure time model for a planar target.

of the reflected beam, and α is the angle between $\boldsymbol{v}_E$ and the propagation direction of the reflected beam. The beam diameter is calculated from the results obtained from the reflected irradiance model. The use of the $1/e^2$ rather than the $1/e$ reflected beam diameter results in a longer (more conservative) exposure time estimate because $D_2 = \sqrt{2}D_1$. This leads to a smaller MPE and a larger RNOHD.

The exposure time model derived in the following is presented in terms of a single time, and to simplify the notation no explicit time dependence is included. When applied to an engagement scenario, with trajectories that are functions of time, the calculations are performed at specific times in the scenario. Also, this model assumes that an observer is located at a distance R in the region illuminated by the reflected beam.

5.1. Model inputs

The major elements of the exposure time model for a plane, cylinder, and cone target are depicted in Figs. 6, 7, and 8, respectively. Inputs required by the exposure time model are the following. The laser, target, and observer are at locations $\boldsymbol{r}_L$, $\boldsymbol{r}_T$, and $\boldsymbol{r}_O$, respectively, with velocities $\boldsymbol{v}_L$, $\boldsymbol{v}_T$, and $\boldsymbol{v}_O$. The orientation of the target is specified by the surface normal $\hat{\boldsymbol{n}}$ for the plane and axis $\hat{\boldsymbol{L}}$ for the cylinder and cone. The derivatives of these quantities with respect to time are also required and are denoted by $\dot{\hat{\boldsymbol{n}}}$ and $\dot{\hat{\boldsymbol{L}}}$. Finally, the cone half-angle is given by γ. Note that in some cases the velocities and orientations must be derived from the positions along a trajectory, whereas in other cases they may be explicitly provided as part of the specification of the trajectory.

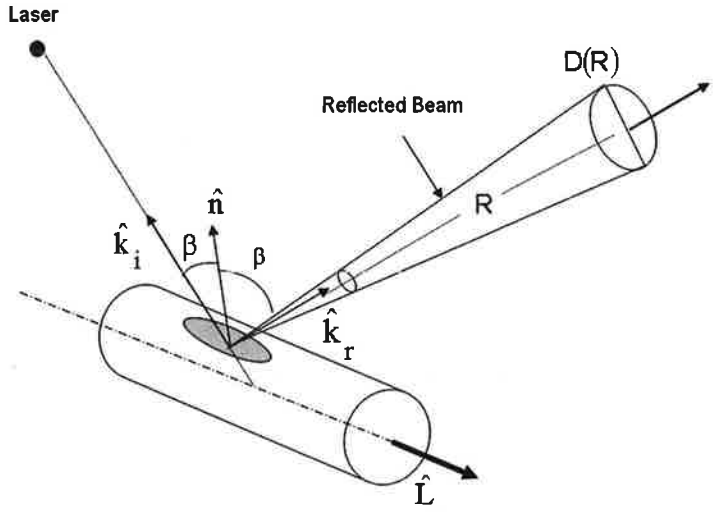

Fig. 7. Geometry for the exposure time model for a cylindrical target.

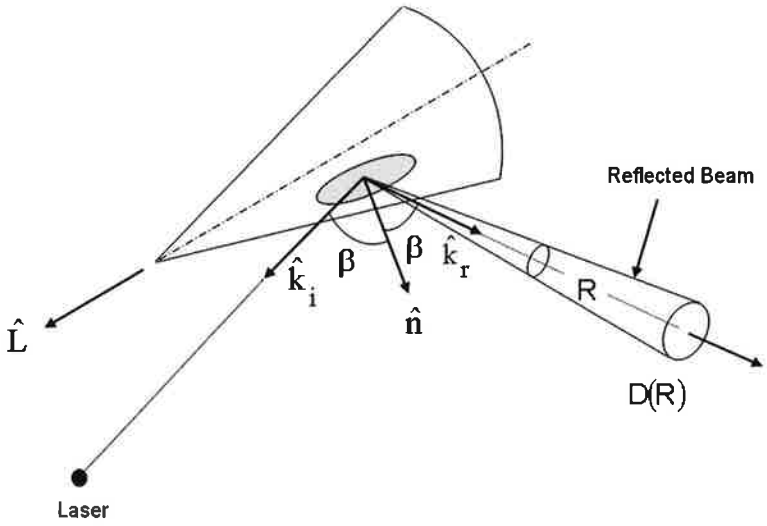

Fig. 8. Geometry of the exposure time model for a conical target.

5.2. Incident beam

The location of the laser relative to the target $\boldsymbol{r}$, its magnitude r, and incident direction $\hat{\boldsymbol{k}}_i$ are given by

$$\boldsymbol{r} = \boldsymbol{r}_L - \boldsymbol{r}_T, \tag{20}$$

$$r = |\boldsymbol{r}|, \tag{21}$$

$$\hat{\boldsymbol{k}}_i = \frac{\boldsymbol{r}}{r}. \tag{22}$$

Similarly, the velocity of the laser relative to the target $\boldsymbol{v}$, its magnitude v, and direction $\hat{\boldsymbol{v}}$ are given by

$$\boldsymbol{v} = \boldsymbol{v}_L - \boldsymbol{v}_T, \tag{23}$$

$$v = |\boldsymbol{v}|, \tag{24}$$

$$\hat{\boldsymbol{v}} = \frac{\boldsymbol{v}}{v}. \tag{25}$$

The angle of incidence β between the incident direction $\hat{\boldsymbol{k}}_i$ and the surface normal of the target $\hat{\boldsymbol{n}}$ is given by

$$\cos\beta = (\hat{\boldsymbol{n}} \cdot \hat{\boldsymbol{k}}_i). \tag{26}$$

For a planar target, the surface normal $\hat{\boldsymbol{n}}_p$ is determined by the geometry of the scenario. For cylindrical and conical targets, however, the surface normal at the location of illumination by the beam depends on the orientation between the incident direction and the axis of the target. The angle θ between the incident direction and the target axis $\hat{\boldsymbol{L}}$, assuming that the incident direction intersects the axis, is given by

$$\cos\theta = (\hat{\boldsymbol{L}} \cdot \hat{\boldsymbol{k}}_i). \tag{27}$$

For a cylindrical target, the surface normal at the location of illumination is given by

$$\hat{\boldsymbol{n}}_{cl} = \frac{\hat{\boldsymbol{k}}_i - \cos\theta\ \hat{\boldsymbol{L}}}{\sin\theta}, \tag{28}$$

whereas for a conical target

$$\hat{\boldsymbol{n}}_c = \frac{\hat{\boldsymbol{k}}_i - \cos\theta\ \hat{\boldsymbol{L}}}{\sin\theta}, \tag{29}$$

$$\hat{\boldsymbol{n}}_{cn} = \cos\gamma\ \hat{\boldsymbol{n}}_c + \sin\gamma\ \hat{\boldsymbol{L}}. \tag{30}$$

The derivative of the incident direction with respect to time $\dot{\hat{\boldsymbol{k}}}_i$ is required in the following and is given by

$$\dot{\hat{\boldsymbol{k}}}_i = \frac{v}{r}\left[\hat{\boldsymbol{v}} - (\hat{\boldsymbol{v}} \cdot \hat{\boldsymbol{k}}_i)\,\hat{\boldsymbol{k}}_i\right]. \tag{31}$$

5.3. Reflected beam

The reflected propagation direction $\hat{\boldsymbol{k}}_r$ is given by

$$\hat{\boldsymbol{k}}_r = 2(\hat{\boldsymbol{n}} \cdot \hat{\boldsymbol{k}}_i)\,\hat{\boldsymbol{n}} - \hat{\boldsymbol{k}}_i = 2\cos\beta\,\hat{\boldsymbol{n}} - \hat{\boldsymbol{k}}_i, \tag{32}$$

which satisfies the condition $(\hat{\boldsymbol{n}} \cdot \hat{\boldsymbol{k}}_r) = (\hat{\boldsymbol{n}} \cdot \hat{\boldsymbol{k}}_i) = \cos\beta$ of specular reflection. The derivative of $\hat{\boldsymbol{k}}_r$ with respect to time $\dot{\hat{\boldsymbol{k}}}_r$ is required to calculate the exposure time, and the expression for this quantity depends on the shape of the target.

For a planar target, because the surface normal and its derivative with respect to time are specified by the scenario, it is easiest to directly differentiate Eq. (32), yielding

$$\dot{\hat{\boldsymbol{k}}}_r = 2\left[(\dot{\hat{\boldsymbol{n}}}_p \cdot \hat{\boldsymbol{k}}_i) + (\hat{\boldsymbol{n}}_p \cdot \dot{\hat{\boldsymbol{k}}}_i)\right] \hat{\boldsymbol{n}}_p + 2(\hat{\boldsymbol{n}}_p \cdot \hat{\boldsymbol{k}}_i)\, \dot{\hat{\boldsymbol{n}}}_p - \dot{\hat{\boldsymbol{k}}}_i. \tag{33}$$

For cylindrical and conical targets, it is convenient to express $\dot{\hat{\boldsymbol{k}}}_r$ in terms of the angle θ rather than β. For a cylindrical target, the angles are related by $\theta \pm \beta = \pi/2$ (+ for $\theta \leq \pi/2$ and – for $\theta > \pi/2$), which yields $\cos\beta = \sin\theta$. Likewise, for a conical target, the angles are related by $\theta + \gamma \pm \beta = \pi/2$ (+ for $\theta + \gamma \leq \pi/2$ and – for $\theta + \gamma > \pi/2$), which yields $\cos\beta = \sin(\theta + \gamma)$.

An additional quantity required for the cylindrical and conical targets is the derivative of Eq. (27) with respect to time, given by

$$\dot{\theta}\sin\theta = -\left[(\dot{\hat{\boldsymbol{L}}} \cdot \hat{\boldsymbol{k}}_i) + (\hat{\boldsymbol{L}} \cdot \dot{\hat{\boldsymbol{k}}}_i)\right]. \tag{34}$$

With the change in angle variable, the expression for $\dot{\hat{\boldsymbol{k}}}_r$ for a cylindrical target is given by

$$\dot{\hat{\boldsymbol{k}}}_r = \dot{\hat{\boldsymbol{k}}}_i + 2\dot{\theta}\sin\theta\ \hat{\boldsymbol{L}} - 2\cos\theta\ \dot{\hat{\boldsymbol{L}}}. \tag{35}$$

The analogous expression for a conical target requires additional algebra, yielding

$$\dot{\hat{\boldsymbol{n}}}_c = \frac{1}{\sin\theta}\left[\dot{\hat{\boldsymbol{k}}}_i - \dot{\theta}\cos\theta\ \hat{\boldsymbol{n}}_c + \dot{\theta}\sin\theta\ \hat{\boldsymbol{L}} - \cos\theta\ \dot{\hat{\boldsymbol{L}}}\right], \tag{36}$$

$$\dot{\hat{\boldsymbol{n}}}_{cn} = \cos\gamma\ \dot{\hat{\boldsymbol{n}}}_c + \sin\gamma\ \dot{\hat{\boldsymbol{L}}}, \tag{37}$$

$$\dot{\hat{\boldsymbol{k}}}_r = 2\dot{\theta}\cos(\theta + \gamma)\ \hat{\boldsymbol{n}}_{cn} + 2\sin(\theta + \gamma)\ \dot{\hat{\boldsymbol{n}}}_{cn} - \dot{\hat{\boldsymbol{k}}}_i. \tag{38}$$

5.4. Exposure velocity

The distance between the target and the observer R is given by

$$R = |\boldsymbol{r}_O - \boldsymbol{r}_T|, \tag{39}$$

and the velocity of the reflected beam $\boldsymbol{v}_R$ is given by

$$\boldsymbol{v}_R = \boldsymbol{v}_T + R \cdot \dot{\hat{\boldsymbol{k}}}_r, \tag{40}$$

where $\dot{\hat{\boldsymbol{k}}}_r$ is calculated from Eq. (33), (35), or (38). The first term in Eq. (40) is a translational contribution due to the motion of the target, and the second term consists of rotational contributions from relative motion between the laser and target and rotation of the target. Note that $\boldsymbol{v}_R$ does not refer to the velocity of the reflected beam along the direction of $\hat{\boldsymbol{k}}_r$, which is the speed of light. Including the velocity of the observer, the resulting velocity of the reflected beam at the observer location $\boldsymbol{v}_E$, its magnitude v_E, and its direction $\hat{\boldsymbol{v}}_E$ are given by

$$\boldsymbol{v}_E = \boldsymbol{v}_O - \boldsymbol{v}_R, \tag{41}$$

$$v_E = |\boldsymbol{v}_E|, \tag{42}$$

$$\hat{\boldsymbol{v}}_E = \frac{\boldsymbol{v}_E}{v_E}. \tag{43}$$

The angle α between this velocity and the reflected direction is given by

$$\cos\alpha = (\hat{\boldsymbol{v}}_E \cdot \hat{\boldsymbol{k}}_r). \tag{44}$$

The quantities calculated from Eqs. (42) and (44) are used in Eq. (19) to calculate the exposure time as a function of distance from the target.

6. RNOHD Calculation

The results from both the reflected irradiance and exposure time models, for a given engagement scenario, are used to calculate the RNOHD, as illustrated in Fig. 1. The exposure time as a function of distance from the target R is used to calculate the MPE as a function of this distance. The reflected irradiance as a function of distance is then compared to the MPE, and the location of intersection is the RNOHD, as given by Eq. (1). In some cases, the MPE is constant with exposure time and an algebraic solution is possible for the RNOHD. In most cases, however, a graphical or iterative solution for the RNOHD is required.

The use of optically aided viewing, such as with binoculars or telescopes, will change the RNOHD relative to the case of unaided viewing. The gain G of an optical system is given by

$$G = \tau \cdot P^2 = \tau \cdot \left(\frac{D_i}{D_e}\right)^2, \tag{45}$$

where τ is the transmittance of the optics, P is the power of the system, and D_i and D_e are the entrance and exit aperture diameters of the system, respectively. The transmittance is 0.9 at visible wavelengths (400–700 nm) and 0.7 at all other wavelengths. There are two equivalent methods for including the gain in the calculation of the RNOHD—either multiply the reflected irradiance by G or divide the MPE by G.

The use of 7×50 binoculars is fairly common. They have a power $P = 7$ and an entrance aperture diameter $D_i = 50$ mm. For a laser at a wavelength of 1.06 μm, the transmittance $\tau = 0.7$. Therefore, the gain $G = 0.7\ (7)^2 = 34.3$ for these binoculars.

7. Example RNOHD Calculations

This section presents an example to illustrate the inputs and calculations required to determine the RNOHD using the methodology detailed in the preceding sections. This example consists of a stationary ground-based laser engaging a target on a parabolic trajectory. The calculations are performed for planar, cylindrical, and conical target shapes. Note that this trajectory is not ballistic but rather is chosen for ease of calculation.

The parabolic trajectory lies in the $x - z$ plane and originates at $x = -5$ km at time $t = 0$ s. The trajectory reaches its apex at $x = -2$ km and $z = 2$ km at $t = 12$ s and terminates at $x = 1$ km at $t = 24$ s. The resulting equations for the x and z locations as a function of time are

$$x(t) = \frac{1}{4}t - 5, \tag{46}$$

Table 1. Inputs of example

Quantity	Laser	Target		
Location	$\boldsymbol{r}_L = (0, 0, 0)$	$\boldsymbol{r}_T = (-1, 1, 16/9)$		
Velocity	$\boldsymbol{v}_L = (0, 0, 0)$	$\boldsymbol{v}_T = (1/4, 0, -1/9)$		
		Plane	Cylinder	Cone
$\hat{n}_p$		$(-0.406, 0, -0.914)$		
$\dot{\hat{n}}_p$		$(-0.038, 0, -0.085)$		
$\hat{L}$			$(0.914, 0, -0.406)$	$(0.914, 0, -0.406)$
$\dot{\hat{L}}$			$(-0.038, 0, -0.085)$	$(-0.038, 0, -0.085)$

$$z(t) = \frac{1}{9}\left(\frac{-1}{8}t^2 + 3t\right). \tag{47}$$

For the planar target, the surface normal $\hat{n}$ is assumed to be perpendicular to the velocity vector, whereas for the cylindrical and conical targets, the axis $\hat{L}$ is parallel to the velocity vector. The laser is stationary at the origin, and the target trajectory is along the line $y = 1$ km. The laser aperture has a diameter $D_{01} = 7$ cm, operates at a wavelength of 1.06 μm, and has an output power of 75 kW, and the resulting beam has an $M^2 = 2$ and is focused at the target. The diameter of the cylindrical target is 12 cm, and the cone target has a half-angle $\gamma = 22.5$ deg and the same base diameter as the cylindrical target. The BRDF of the target material results is $\phi_m = 2.5$ mrad and the reflectance $\rho = 1$. The RNOHD is evaluated at time $t = 16$ s, corresponding to a distance from the laser to the target of 2.3 km and an altitude of 1.8 km. The resulting inputs required for the analysis are given in Table 1.

The values of the quantities relevant for each model are given in Table 2, along with the numbers of the equations used for the calculation. Both the reflected irradiance and the exposure time depend on the distance R from the target to the observer. The reflected irradiance is determined using Eq. (16), the stated reflectance of the target material and the power of the laser, and $\phi_{//}$ and $\phi_{\perp}$ calculated using the values of ϕ_b, ϕ_m, and ϕ_{c1} in Table 2. The exposure time T is determined by applying Eqs. (36)–(42) using the appropriate k_r for each target shape and D_2 calculated using ϕ_{ce} in Table 2 and assuming that the observer is stationary so $\boldsymbol{v}_O = (0, 0, 0)$. For a laser wavelength of 1.06 μm, the MPE for exposure times greater than 50 μs is given by

$$\text{MPE} = 90 \cdot T^{-0.25}\ \text{W/m}^2. \tag{48}$$

Plots of both reflected irradiance and MPE as a function of distance from the target are shown in Figs. 9–11 for the planar, cylindrical, and conical target, respectively. The distance at which the reflected irradiance equals the MPE is also indicated in each figure as the RNOHD. Because the RNOHD for the cylindrical and conical targets is less than the altitude (1.8 km), there is no hazard on the ground under these specific conditions. To complete this example, aided viewing using 7×50 binoculars increases the RNOHDs to 45, 3.1, and 2.1 km for the planar, cylindrical, and conical targets, respectively.

Table 2. Calculated quantities of example

Quantity	Eq.	Plane	Cylinder	Cone
Beam propagation model				
D_{t1} (cm)	(3)	4.4	4.4	4.4
Reflected irradiance model				
ϕ_b (mrad)	(8)	0.03	0.03	0.03
ϕ_m (mrad)		2.5	2.5	2.5
ϕ_{c1} (rad)	(11)	0	1.5	3.3
ϕ_{ce} (rad)	(14)	0	1.2	1.6
Exposure time model				
$\hat{\boldsymbol{k}}_i$	(22)	(0.440, −0.440, −0.783)	(0.440, −0.440, −0.783)	(0.440, −0.440, −0.783)
$\hat{\boldsymbol{v}}$	(25)	(−0.914, 0, 0.406)	(−0.914, 0, 0.406)	(−0.914, 0, 0.406)
$\cos\theta$	(27)		0.720	0.720
$\hat{\boldsymbol{n}}_{cl}$	(28)		(−0.314, −0.634, −0.706)	
$\hat{\boldsymbol{n}}_c$	(29)			(−0.314, −0.634, −0.706)
$\hat{\boldsymbol{n}}_{cn}$	(30)			(0.060, −0.586, −0.808)
$\cos\beta$	(27)	0.536	0.694	0.917
$\dot{\hat{\boldsymbol{k}}}_i$	(31)	(−0.072, −0.038, −0.019)	(−0.072, −0.038, −0.019)	(−0.072, −0.038, −0.019)
$\hat{\boldsymbol{k}}_r$	(32)	(−0.876, 0.440, −0.198)	(−0.876, −0.440, −0.198)	(−0.331, −0.634, −0.699)
$\dot{\hat{\boldsymbol{k}}}_r$	(33)	(−0.047, 0.038, −0.248)		
$\dot{\theta}\sin\theta$	(34)		0.00822	0.00822
$\dot{\hat{\boldsymbol{k}}}_r$	(35)		(−0.0026, −0.038, 0.096)	
$\dot{\hat{\boldsymbol{n}}}_c$	(36)			(−0.050, −0.047, 0.064)
$\dot{\hat{\boldsymbol{n}}}_{cn}$	(37)			(−0.060, −0.044, 0.027)
$\dot{\hat{\boldsymbol{k}}}_r$	(38)			(−0.038, −0.047, 0.061)

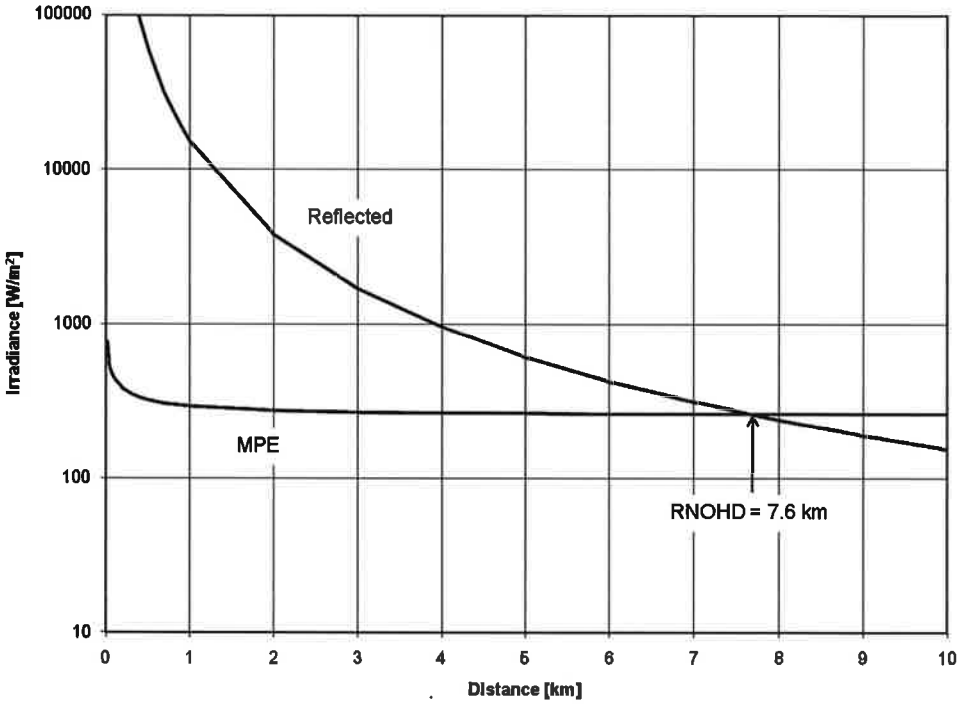

Fig. 9. Reflected irradiance and MPE as a function of distance from the target, and the RNOHD, for the example with a planar target.

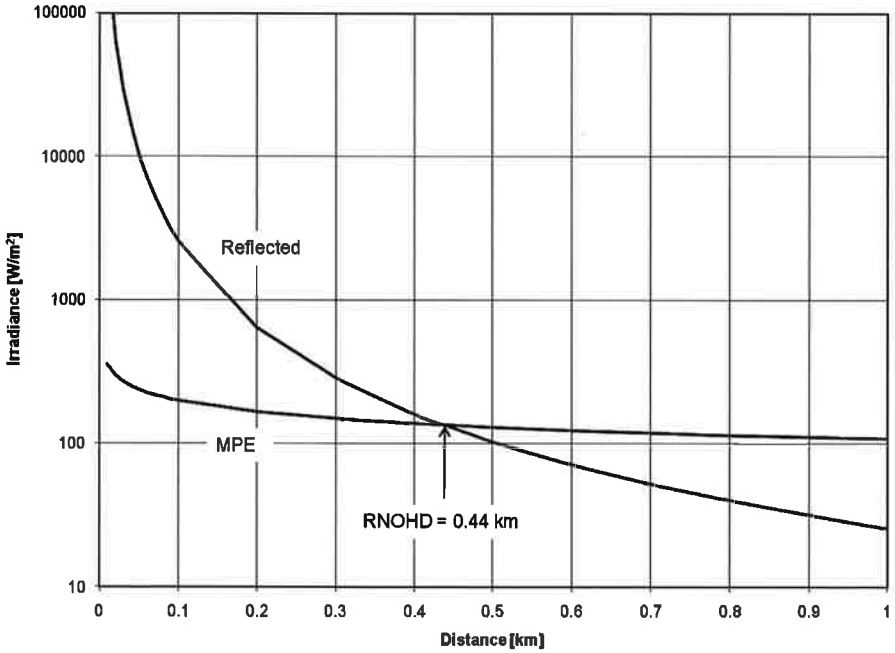

Fig. 10. Reflected irradiance and MPE as a function of distance from the target, and the RNOHD, for the example with a cylindrical target.

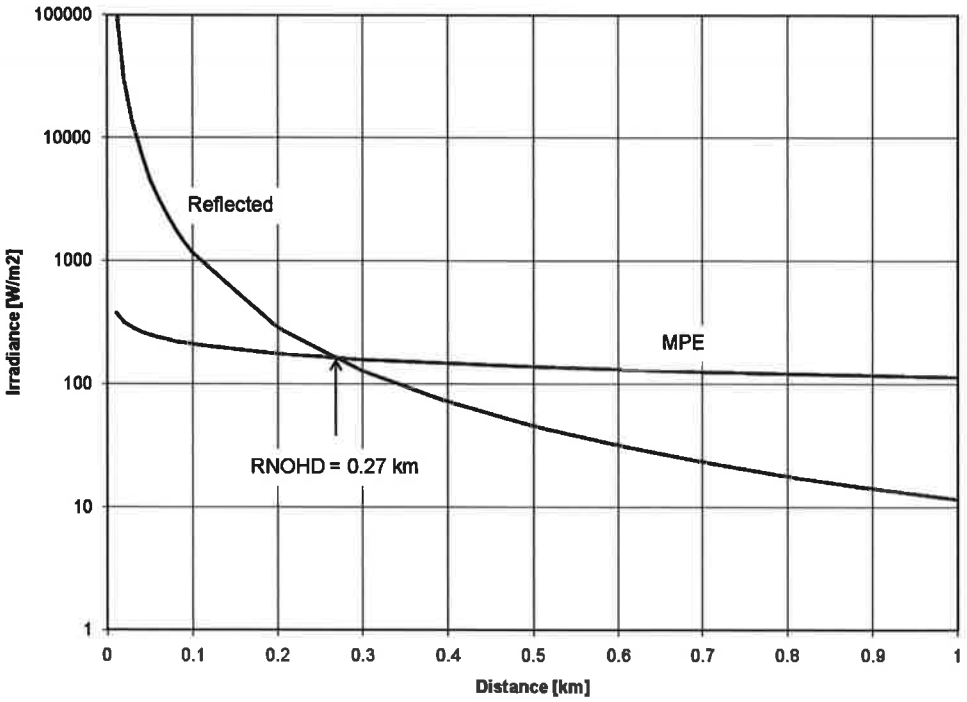

Fig. 11. Reflected irradiance and MPE as a function of distance from the target, and the RNOHD, for the example with a conical target.

Table 3. RNOHDs of example calculated using two methodologies

	RNOHD (km)	
Target	Methodology of this paper	Overly conservative methodology
Plane	7.6	1,450
Cylinder	0.44	4.2
Cone	0.27	2.8

It is instructive to compare the RNOHDs obtained using different techniques. One such technique is the overly conservative methodology, which motivated the methodology detailed in this paper. The overly conservative methodology uses a 10-s exposure time, corresponding to the lowest MPE, and does not include the BRDF of the target material. The RNOHDs obtained using these two methodologies are listed in Table 3 for this example. The overly conservative methodology yields RNOHDs that are significantly longer than those obtained using the methodology of this paper, particularly in the case of a planar target. For the cylindrical and conical targets, the shape contributes to the divergence of the reflected beam, so the differences between RNOHDs using the two techniques are not as pronounced.

The other technique to consider is diffuse reflections, which is a counterpoint to the use of specular reflections in the methodologies of the preceding paragraph. The RNOHD for

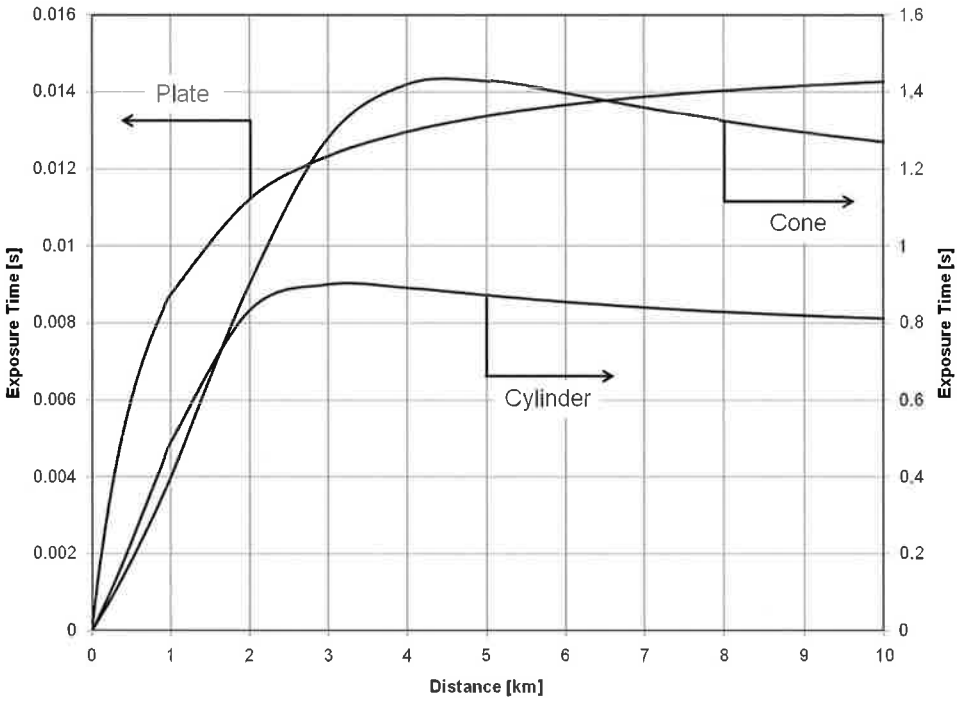

Fig. 12. Exposure time for the example for each indicate target.

diffuse reflections is given by

$$\text{RNOHD} = \sqrt{\frac{\rho}{\pi}\frac{\Phi \cdot \cos\theta_V}{\text{MPE}}}, \tag{49}$$

where θ_V is the viewing angle. For this example, $\theta_V = 0$ deg, $\rho = 1$, and the MPE corresponding to a 10-s exposure time were used in Eq. (49) to calculate RNOHD = 22 m. This is much shorter than for specular reflections, which further justifies their use in the methodology detailed in this paper.

Returning to the results shown in Figs. 9–11, the RNOHD is much longer for the planar target than for the cylindrical or conical targets. The larger divergence of the reflected beam for the latter two targets increases the exposure time compared to that of the planar target, resulting in a lower MPE. However, this effect is more than offset by the decreased reflected irradiance, also due to the larger divergence. A plot of the exposure times as a function of distance from the target is shown in Fig. 12. For the plate, the exposure times are on the order of several milliseconds, whereas for the cone and cylinder the exposure times are approximately 200 ms at the RNOHD and increase to roughly 1 s at greater distances. In very simple engagement scenarios (e.g., only the laser moves), the exposure time merely depends on the reflected beam divergence and is therefore constant with distance from the target. However, the exposure time in the example presented in this section has a more complicated dependence on distance, even being nonmonotonic for the cylinder and cone, although all exposure times will become constant at sufficiently long distances.

8. Conclusions

Overly conservative assumptions applied to safety analyses of HEL beam reflections from targets often result in hazard zones that are not contained within test range boundaries. The reflected beam hazard analysis methodology presented in this paper was developed to address the need for a less conservative and more accurate procedure for estimating RNOHDs to support HEL field tests. The primary goal was to provide laser safety analysts the tools necessary to evaluate potential reflected beam hazards and design HEL field tests that conform to current laser safety procedures.

The methodology consists of several physically based models and is applicable to engagement scenarios in which a single laser illuminates a target, with both the laser and target moving along independent trajectories. A beam propagation model is used to calculate the properties of the incident beam at the target location. A reflected irradiance model uses the properties of the incident beam, the target shape, and the BRDF of the target material to determine the reflected irradiance as a function of distance from the target. The methodology also includes an exposure time model that calculates the time during which an observer is exposed to the reflected beam. The exposure time model takes into account the position, velocity, and orientation of both the target and the laser. In summary, the methodology provides a unified framework for calculating more accurate RNOHD values than those obtained with overly conservative assumptions.

References

[1]American National Standards Institute, *American National Standard for Safe Use of Lasers Outdoors, ANSI Standard Z136.6–2005*, Laser Institute of America, Orlando, FL (2005).

[2]American National Standards Institute, *American National Standard for Safe Use of Lasers, ANSI Standard Z136.1–2007*, Laser Institute of America, Orlando, FL (2007).

[3]Bailey, A.W., E.A. Early, K.S. Keppler, V.I. Villavicencio, P.K. Kennedy, R.J. Thomas, J.J. Zohner, and G. Megaloudis, J. Laser Appl. **20**, 22 (2008).

[4]Keppler, K., G. Megaloudis, E. Early, P. Kennedy, and R. Thomas, "Reflected Laser Hazard Analysis Methodology to Support HEL Field Testing," DoD Technical Report No. AFRL-RH-BR-TR-2008-0029, U.S. Air Force Research Laboratory, Brooks City-Base, TX (2008).

[5]Maxwell, R.J., J. Beard, S. Weiner, D. Ladd, and S. Ladd, "Bi-directional Reflectance Model Validation and Utilization," DoD Technical Report No. AFAL-TR-73-303, Environmental Research Institute of Michigan, Ann Arbor, MI, and Air Force Avionics Laboratory, Wright–Patterson Air Force Base, OH (1973).

[6]Sliney, D., and M. Wolbarsht, *Safety with Lasers and Other Optical Sources*, Plenum Press, New York, p. 126 (1980).

[7]Thomas, R.J., B.A. Rockwell, W.J. Marshall, R.C. Aldrich, M.F. Gorschboth, S.A. Zimmerman, and R.J. Rockwell, J. Laser Appl. **16**, 167 (2004).

[8]Thomas, R.J., B.A. Rockwell, W.J. Marshall, R.C. Aldrich, M.F. Gorschboth, S.A. Zimmerman, and R.J. Rockwell, J. Laser Appl. **19**, 46 (2007).

[9]Thomas, R.J., B.A. Rockwell, W.J. Marshall, R.C. Aldrich, S.A. Zimmerman, and R.J. Rockwell, J. Laser Appl. **13**, 134 (2001).

[10]Thomas, R.J., B.A. Rockwell, W.J. Marshall, R.C. Aldrich, S.A. Zimmerman, and R.J. Rockwell, J. Laser Appl. **14**, 57 (2002).

The Authors

Dr. Edward Early received a B.S. degree in physics from Texas A&M University in 1984 and M.S. and Ph.D. degrees in physics from the University of California, San Diego, in 1987 and 1991, respectively. Following a postdoctoral position in high-temperature

superconductor research, he joined the Optical Technology Division of the National Institute of Standards and Technology, where he worked on standards and calibrations for spectrophotometry, color and appearance, and remote sensing. He joined TASC in 2004 and currently supports the Optical Radiation Branch of the Air Force Research Laboratory in the area of high-energy-laser safety analyses, specifically developing analysis techniques and researching reflecting properties of materials at high temperatures. He is a member of DEPS, OSA, and ANSI.

Dr. Paul Kennedy received B.S., M.S., and Ph.D. degrees in physics from North Texas State University in 1976, 1980, and 1983, respectively. In 1983 he joined the Rocketdyne Division of Rockwell International, where he served as a theoretical analyst and scientific programmer supporting research and development on high-energy lasers. Since 1992 he has been a Senior Research Biophysicist in the Optical Radiation Branch of the Air Force Research Laboratory, characterizing and modeling the interaction of lasers and other optical radiation with biological systems, primarily the eyes and skin. In this capacity he has developed theoretical models and performed numerous analytical studies to predict laser-induced tissue damage and its effect on military operations. He is currently a senior scientist and technical advisor to the USAF High Energy Laser Safety Program. He is a member of APS, OSA, DEPS, and SPIE

Dr. George Megaloudis received B.A. and Ph.D. degrees in physics from Northeastern University in 1970 and 1977, respectively. Since 1981 he has been with TASC, where he has performed technical analyses and prototype system design in a broad range of technologies. These include remote sensing, RF and electro-optical active and passive sensors, signal processing, statistical analysis, pattern recognition, numerical simulation, and atmospheric phenomenology. Currently, he performs laser safety analyses to support high-energy-laser field tests. In this capacity, he developed theoretical models and several prototype tools to predict the properties of high-energy-laser radiation reflected from real-world targets.

Dr. Robert J. Thomas received his B.S. degree in physics in 1989 from Pittsburg State University, Kansas, and his Ph.D. in physics in 1994 from the University of Missouri. He is currently a physicist in the Optical Radiation Branch of the Air Force Research Laboratory. He has worked for the past 15 years in the field of laser–tissue interactions, with an emphasis on numerical simulations. He is a member of SPIE, IEEE, and the American Physical Society, as well as a Fellow of the Laser Institute of America.